Industrial distortion index assessment for a boundary layer ingestion engine

Hector Solorzano Flores, Cyril Bonnaud, Alain Dega, Ludovic Gerard, Olivier Atinault, Julien Dandois

Industrial distortion index assessment for a boundary layer ingestion engine

Hector Solorzano[1], Cyril Bonnaud[2], Alain Dega[3] and Ludovic Gerard[4]
Airbus Operations SAS, 316 route de Bayonne, Toulouse, 31060, France

Olivier Atinault[5] and Julien Dandois[6]
DAAA, ONERA, Université Paris Saclay, 8 rue des Vertugadins, Meudon, 92190, France

A possible solution to improve the aircraft efficiency for the next decades is the use of boundary-layer ingestion engines. One of the industrial challenges linked to this type of engines is the aerodynamic distortion at engine intake. This work proposes to evaluate the characterization capability of several distortion indices, currently used in the industry, on a boundary layer ingestion engine configuration. The analysis is performed using several Reynolds-Averaged Navier-Stokes simulations. First, steady simulations of a simplified boundary-layer ingestion air intake are performed for off-design conditions. The principal distortion indices used in the industry are calculated for each flow solution. The results are discussed to assess their potential to highlight physical phenomena present in this configuration. Finally, this analysis allows identifying the weaknesses of the current distortion indices and to propose ways of improvement for new distortion indices more adequate for boundary layer ingestion configurations.

I. Nomenclature

α	=	swirl angle
BLI	=	boundary-layer ingestion
β	=	relative angle of attack
βIDC	=	circumferential distortion index based on the relative angle of attack
CFD	=	computational fluid dynamics
$DC(\theta)$	=	distortion descriptor in lowest stagnation pressure θ degree sector
IDC	=	circumferential distortion index
MFR	=	mass flow rate
P	=	stagnation pressure
q_f	=	average dynamic pressure
RANS	=	Reynolds-Averaged Navier-Stokes
SI	=	swirl intensity
VPDI	=	velocity and pressure distortion index

[1] PhD Student, Component Aerodynamics Department.
[2] Aerodynamics Engineer, Component Aerodynamics Department.
[3] Aerodynamics Engineer, Component Aerodynamics Department.
[4] Aerodynamics Engineer, Component Aerodynamics Department.
[5] Research Scientist, Department of Aerodynamics, Aeroelasticity, Acoustics.
[6] Research Scientist, Department of Aerodynamics, Aeroelasticity, Acoustics.

II. Introduction

The main objective in new aircraft design is the improvement in energy efficiency, which is linked to a commitment to reduce the environmental impact of aviation, as well as operating costs. An interesting option for designing more efficient aircraft is to increase the synergy between its components. Boundary-Layer Ingestions (BLI) aircraft concepts, such as Aurora D8 [1] [2], NASA STARC-ABL or ONERA NOVA-BLI [3] appear to be promising solutions. These concepts are based on improving the interaction between the fuselage and the propulsion systems in such a way that the latter ingests the viscous boundary layer or fuselage wake.

Figure 1 - ONERA NOVA concept

This potential solution brings some design problems that do not allow to meet some engine requirements. One of the requirements is focused notably on the flow homogeneity at the engine intake. The flow heterogeneity, named distortion, may account for the appearance of aerodynamic instabilities of the fan blades. If the distortion is large enough, the fan might stall or the engine may surge. During the design phase, an index to measure the distortion is necessary to define the fan tolerance to perturbations on the ingesting flow. There are several indices used in the industry to characterize the distortion at engine intake. Most of these indices were designed to analyze the distortion in a standard engine configuration and are based on stagnation pressure losses. Several authors have made theirs distortion analysis and performance prediction for a BLI engine by using these typical distortion indices [4] or using a pressure-based distortion criteria [5] [6]. Probably these distortion indices are not suitable for use in a BLI engine configuration, especially knowing that the physical phenomena of a BLI engine are different from an engine in a standard configuration.

This work aims to assess the common distortion indices used in the industry on a BLI engine. For this analysis, CFD simulations are performed by using several Reynolds-Averaged Navier-Stokes turbulence models. The most distorted flow appears when the aircraft is flying in off-design conditions; in this case a low mass-flow rate and a high free stream velocity are encountered. In the industry, the most used distortion indices are the IDC and DC(θ), both based on stagnation pressure. In addition to these indices, an interesting methodology for assessing the inlet distortion swirl [7] is evaluated for a BLI engine application. An individual analysis of each distortion index is performed. These analysis allows to highlight their weaknesses and strengths by representing the physical phenomena on a BLI engine. Then, some new lines of research to improve a distortion index for a BLI engine are proposed.

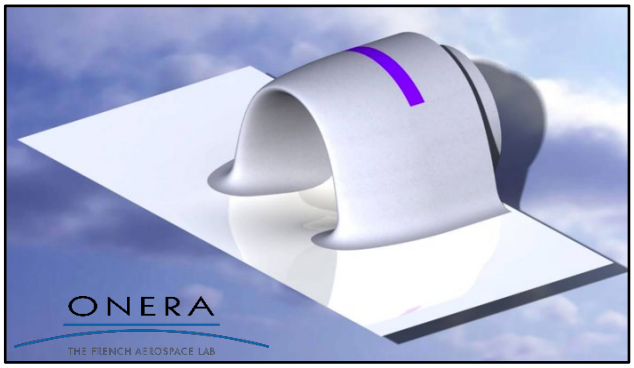

Figure 2 – Inlet model

Figure 2 shows the geometry used. This work does not take into account the effect, or possible impact, on internal engine components, only the inlet is modeled. In the future, it is expected to complement and compare this work with experimental results, therefore, this geometry has been taken from a model designed to be analyzed in a wind tunnel campaign, which is contemplated in the same project.

III. Analysis Method

A. CFD Simulations

In order to analyze the distortion indices several CFD simulations are performed. These analyses are made from an industrial point of view, using linear as well as non-linear eddy viscosity turbulence models.

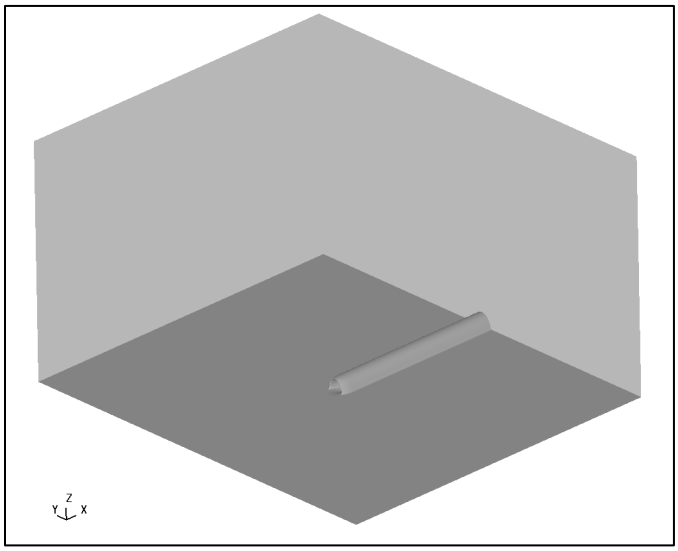

Figure 3 - Simulation domain

The simulations are carried out using elsA [8], an Airbus-ONERA-Safran CFD solver. RANS simulations are performed, with first and second order turbulence models used to solve the Reynolds stress tensor term. The Spalart-Allmaras and k-ω SST models are well-known and used for most of the aeronautical applications. In addition, the SA-RC and SA-QCR2000 modification for the standard Spalart-Allmaras model are considered for the analysis. The SA-RC correction is designed to improve the accuracy by taking into acc ount rotation and curvature effects [9]. The SA-QCR2000 model is computed like in the original SA, but instead of the traditional linear Boussinesq relation, a second non-linear term to the linear Reynolds stress tensor is added [10]. Finally, a SSG/LRR full Reynolds Stress Model is also used. According to the bibliography [11], the RSM models exhibit several advantages when simulating turbulent flows at high Reynolds numbers with secondary effects. The inclusion of such a diverse set of models allows for a comparison of the differences in the physical phenomena predicted and their impact on the distortion criteria.

All the simulations performed are steady. They are solved using Jameson's second-order-accurate central scheme with artificial viscosity for the spatial discretization. The second and the fourth-order dissipation coefficient are equal to 0.5 and 0.016 respectively. The artificial viscosity reduction uses a e^2 value. For the turbulent equations, a Roe scheme coupled with Harten's formulation with velocity term $|u| + |v| + |w| + c$, its coefficient value is 0.01. All the simulations are calculated for a fully turbulent and steady solution by using a Courant–Friedrichs–Lewy number between 10 and 50.

The configuration chosen for the study is a semi-buried BLI intake placed on the aft fuselage side and ingesting the boundary layer developing along the fuselage, as shown in Figure 1. Figure 2 shows the simplified geometry, which consist on an air intake half-buried in a flat plate. The fan diameter is D = 164mm. The external and the rear shape have been designed taking into account the set up constraints of the model in the wind tunnel. The farfield boundary conditions are placed at 20D. The domain shape is a cube with 40D length on each side. Figure 3 shows the simulation domain

The overall grid has about 24 million elements. It is a structured multi-block mesh consisting of hexagonal elements. Inside the intake, an OH-grid topology is used. The outside of the intake is formed by a mixture of C-grid near the intake and the O-grid extending outward, as shown in Figure 4. A mesh convergence study has been performed to make sure that the solution is not mesh dependent.

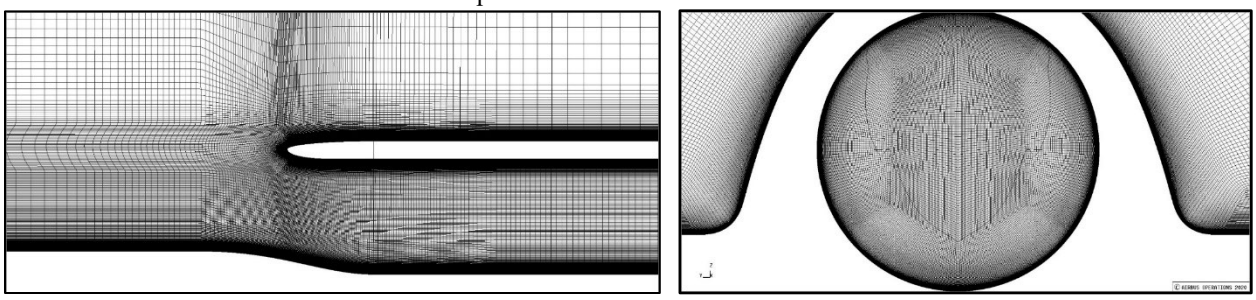

Figure 4 - Mesh topology

Once the mesh independence of the result can be assured, the analysis of physical phenomena is the next step. The use of a BLI engine means that the fan input is guaranteed to be distorted due the boundary layer thickening. This distortion could increase when operating in off-design conditions. It is planned to replicate and analyze these conditions in the wind tunnel. The flow conditions chosen for the simulations are the same as expected in the wind tunnel. A transonic Mach number (Mach = 0.82) for the free stream and a variation of the mass flow rate *MFR* passing through the engine is studied. . The simulations are steady. The flow at freestream is parallel to the flat plane and has zero sideslip angle. The static temperature is 310 k and the Reynolds number is 13.1 million. For low MFR values, the appearance of a separated flow is expected

The residuals of the continuity equation and the turbulence equations are used as the convergence criteria. In all cases, these residues decrease by several orders of magnitude. The MFR is monitored both on the fan face and on the surface in which the boundary condition is applied. In addition, the lift and drag values integrated on the nacelle surface are used as a physical parameter to monitor the convergence. The case matrix of the simulations is presented in table 1. Blue cases are the ones for which a separated flow is observed, green cases are attached flow. Details of the turbulence models used can be found in the references [9] [10] [11] [12] [13][14].

Turbulence Model / MFR	3.0 kg/s	3.2 kg/s	3.4 kg/s	3.5 kg/s	3.6 kg/s	3.7 kg/s	4.0 kg/s
Spalat Allmaras (SA)							
SA with Rotation/Curvature Correction (SA-RC)							
SA with Quadratic Constitutive Relation (SA-QCR2000)							
k-ω with Standard Menter SST Two-Equation Model (k-ω SST)							
SSG/LRR Full Reynolds Stress Model (RSM)							

Table 1 - Matrix Cases

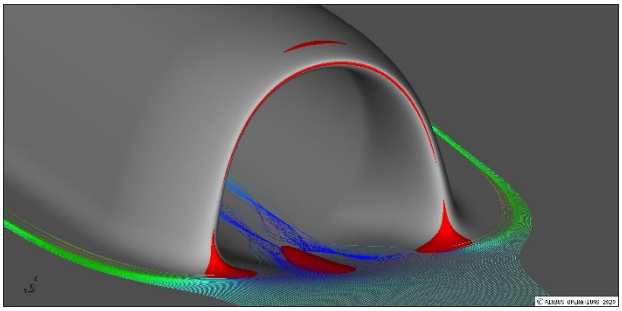

Figure 5 - Flow solution - MFR = 3.2 kg/s

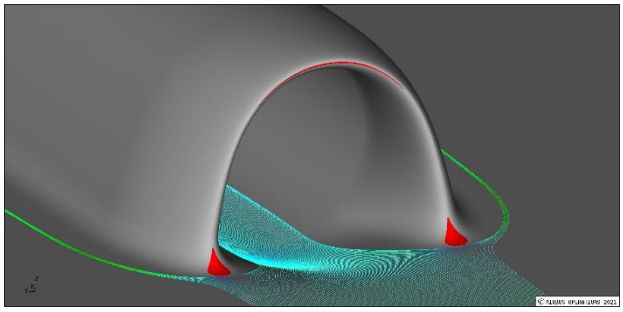

Figure 6 - Flow solution - MFR = 4.0 kg/s

As expected, all simulations shows a clear interaction between the fuselage, represented as a flat plane, and the BLI intake. The main question is how to quantify this distortion generated and its impact on engine performance. Before performing a distortion measure, it is necessary to understand the flow and identify the main mechanisms that generate it.

Figures 5 and 6 show the typical flow behavior predicted for two different MFR values. The red iso-surfaces show areas of negative axial velocities, which serve to identify areas of separated flow. The separated main area is located at the bottom of the engine intake. As expected, this region of separation is due to an adverse pressure gradient at low MFR, as shown in figure 5. This separation does not occur when the pressure gradient decreases, as shown in Figure 6. The appearance of this separation occurs between 3.4 and 3.5 kg/s depending on the turbulence model used. This separation zone impacts negatively the homogeneity of the flow. Both the total pressure and the axial velocity decrease in the affected region, adding to the adverse effect of the ingestion of the boundary layer. Another important physical phenomenon is the creation of counter-rotating vortices at engine intake, their presence is obvious in Figure 5 (in blue). The generation of these vortices is independent of the presence of separation. This physical phenomenon is

present in all cases. These vortices also negatively affect the flow homogeneity creating tangential and radial velocities which, in principle, are not desired as a flow condition.

Figure 7 and Figure 8 show the total pressure and axial velocity at engine intake and symmetric plane. These two parameters have a direct impact on the engine performance. Most of the distortion criteria used in industry are based on one of these two parameters. In the next section these distortion criteria are presented, and their sensibility to the physical phenomena highlighted in this section are evaluated.

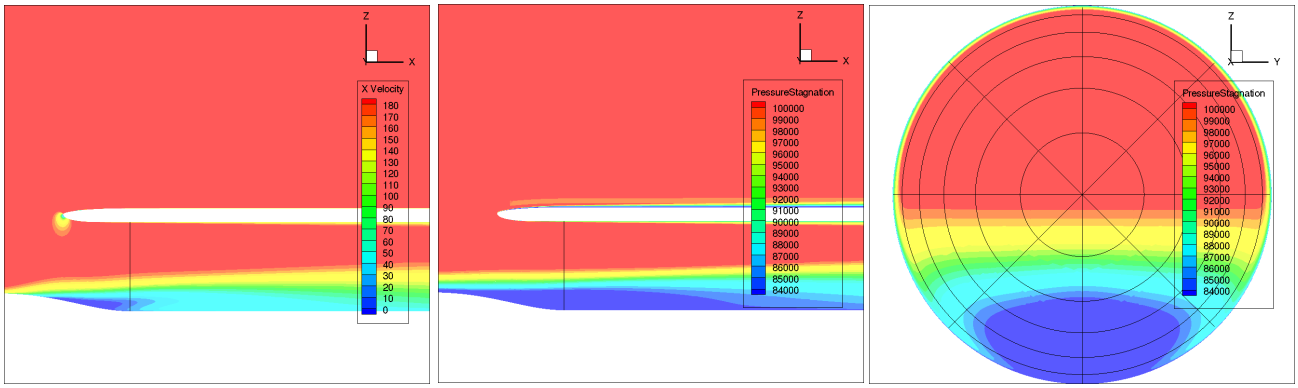

Figure 7 – Axial Velocity and Total Pressure - MFR = 3.2 kg/s

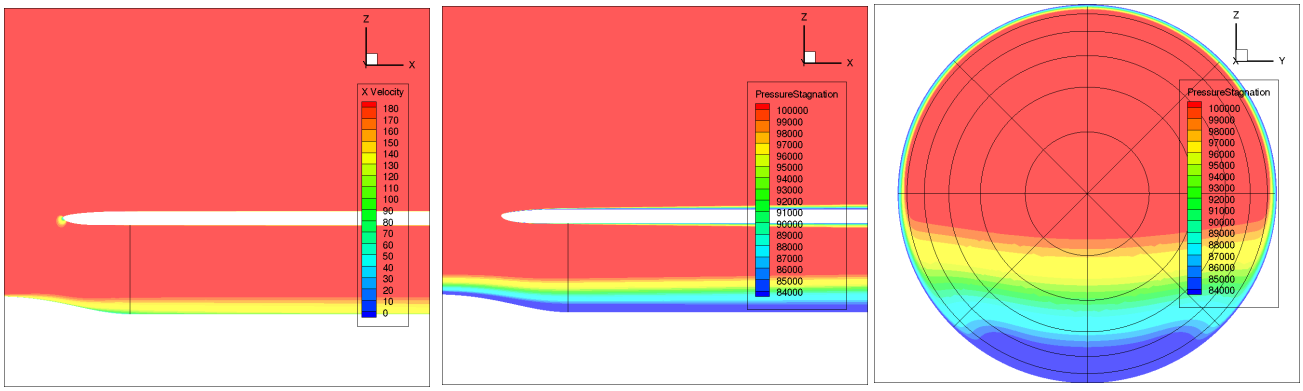

Figure 8 - Axial Velocity and Total Pressure - MFR = 4.0 kg/s

B. Industrial distortion indices

The distortion criteria analyzed in the present study are the most common ones used to characterize the distortion at the industry. First, the well-known *IDC* and $DC(\theta)$ indexes are described. Reference [15] proposes interesting distortion criteria by using the radial and circumferential distortion intensity. All distortion indices mentioned so far are based on pressure measurements, and were developed to be used in experimental tests.

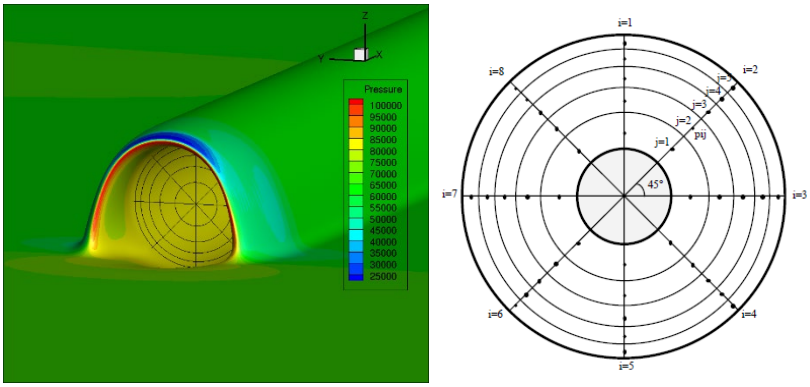

Figure 9 – Rake at fan face

The BLI engine intake solution exhibits also very important velocity gradients, both in axial and tangential directions. Therefore, distortion criteria based on velocity are included in this work. Reference [7] shows a methodology for assessing inlet swirl distortion. By using this methodology some stationary swirl distortion indices are proposed.

The indices are designed, in general, to be used in experimental test, therefore the simulation measurements are taken by using the rake placed at the fan face shown in figure 9. This rake is composed of eight arms with 45° between them. Each arm have five measurement points. Depending on the distortion criteria, the static pressure, stagnation pressure, or velocity, are the measured parameters in stationary conditions.

IV. Results and discussion

In this section some distortion indices are calculated and evaluated. A priori, the distortion criteria can be divided into two groups directly linked to a flow parameter. The effect of the turbulence models on the solution and the distortion indices is analyzed.

A. Pressure based distortion criteria

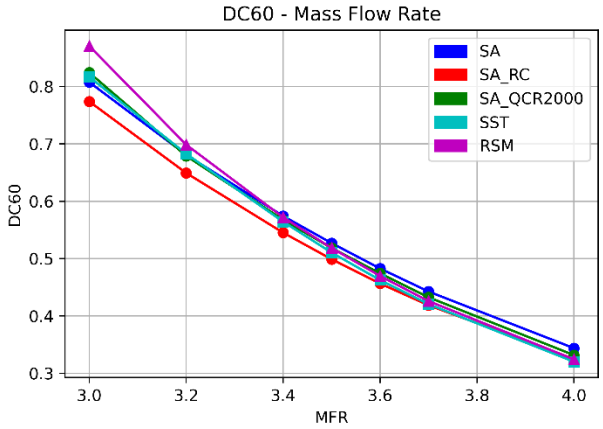

Figure 10 - DC(60) variation with MFR value

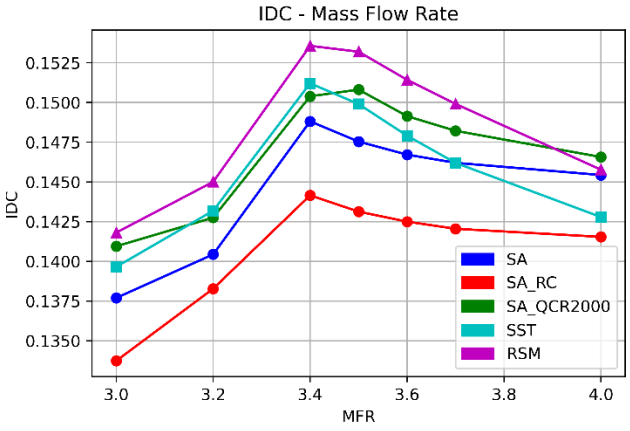

Figure 11 - IDC variation with MFR value

$$\mathbf{DC(\theta)} = \frac{\overline{P_f} - \overline{P_\theta}}{q_f} \qquad \textbf{Equation 1}$$

The ***DC(θ)*** is defined by Equation 1. The most distorted region of 60° is used for this index. The values measured in the solutions are shown in Figure 10. The plot shows that this index tends to decrease almost linearly with the mass flow rate value. At first it was expected that the *DC(60)* decrease would be linear until it reaches a mass flow rate value for which there is no more detached flow. However, there is no change in the behavior of this index. This linear evolution is due to the variation of the momentum at the fan face (q_f) which increases with the mass flow rate and to the difference between the mean stagnation pressure at the fan face and the mean stagnation pressure for a 60° sector ($P_f - P_\theta$) which have the same evolution. The *DC(60)* value will continue to decrease until the engine mass flow rate reaches sonic conditions.

The **IDC** (Circumferential Distortion Index) takes into account the pressure distribution across the circumference. Its value is given by Equation 2. Figure 11 shows its value at each simulation case. The IDC value shows a quite interesting correlation with the flow separation, since its value is maximum for the mass flow rate value for which the separation triggers. This implies that this index could be used to detect the mass flow rate for which a separation appears. The IDC measures the difference of circumferential distortion between

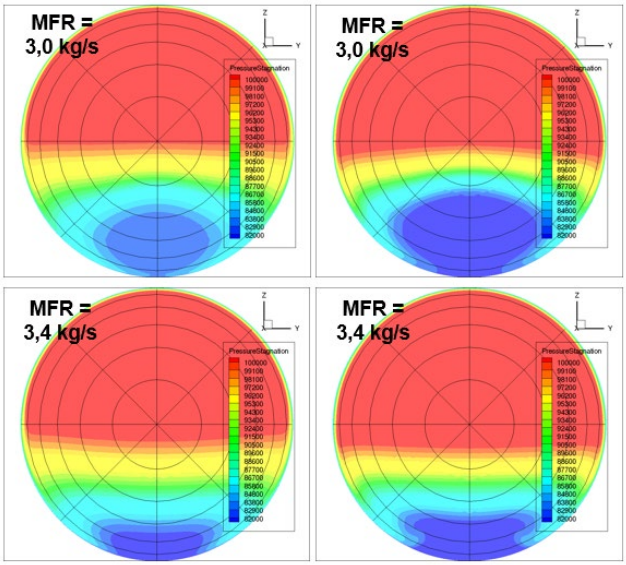

Figure 12 - Total pressure value at fan face

Left: SA-RC model. Right: RSM model

neighboring circles and in the case where the separation appears, this value is maximum because there is only a small area with a low stagnation pressure. Figure 12 shows the total pressure field at fan face for some simulation cases.

It can be noticed that the results obtained for the pressure-based distortion indices do not fully correlate with the physical phenomena present in the cases studied. Figures 7 and 8 show the total pressure at fan intake, the first shows a fully separated flow ($3.2\ kg \cdot s^{-1}$) and the second shows a non-separated flow ($4.0\ kg \cdot s^{-1}$). In both cases the percentage of the impacted region by the decrease in total pressure are similar, instead, the region with the lowest total pressure is more localized and far from the geometric center when the flow is attached. This behavior is also evident in figure 12. This explains the better correlation with the physics presented by the IDC, and the low correlation for the DC(60).

$$IDC = MAX_{i=1}^{nradius-1}\left(0.5\left[\frac{(\overline{P_i}-\overline{Pmin_i}}{\overline{P}_f}+\frac{(\overline{P_{i+1}}-\overline{Pmin_{i+1}}}{\overline{P}_f}\right]\right) \quad \textbf{Equation 2}$$

B. Velocity based distortion criteria

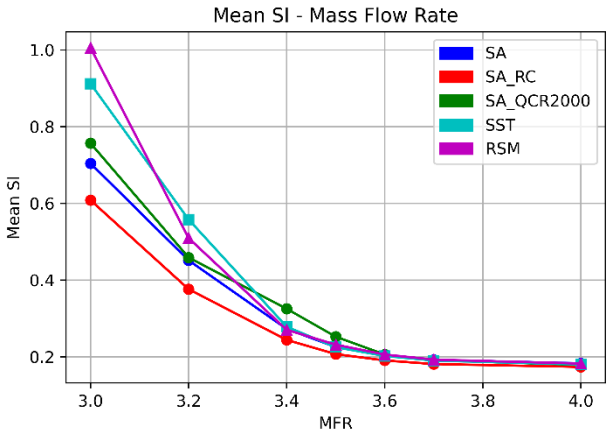

Figure 13 - Mean SI variation with MFR value

The **Swirl Intensity (SI)** is an interesting parameter to characterize the distortion [7]. The SI index is defined as the "extent weighted" absolute swirl, and this value is calculated at each measurement ring (j index) on the rake. The i index means the azimuthal position.

$$SI_j = \frac{SS_j^+ \times \theta_j^+ + |SS_j^-| \times \theta_j^-}{360} \quad \textbf{Equation 3}$$

$$SS_j^{\pm} = \int_{\theta_j^{\pm}} \frac{\alpha(\theta)_j}{\theta_j^{\pm}} d\theta$$

$$\alpha_i = tan^{-1}\left(\frac{V_t}{V_x}\right)_j$$

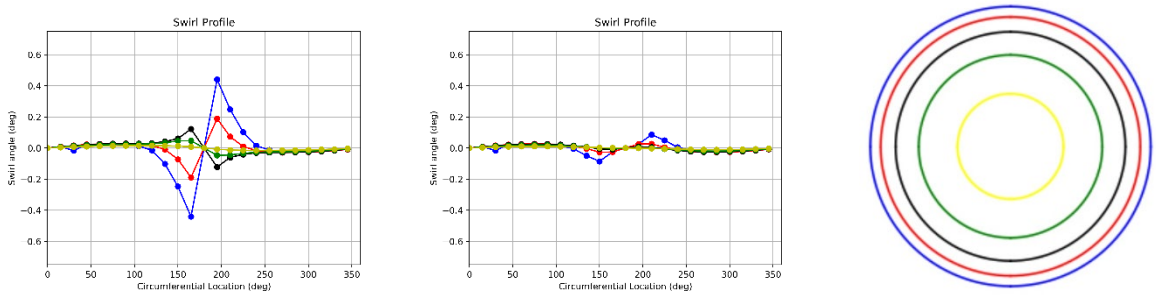

Figure 14 - SI values. Left: MFR = 3.2 kg/s. Center: MFR = 4.0 kg/s.

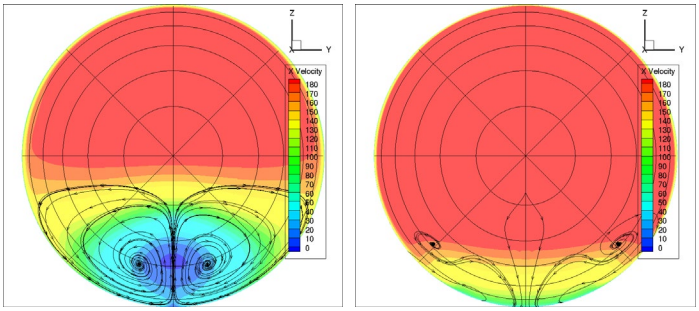

Figure 15 - Streamlines at fan face.

Left: MFR = 3.0 kg/s. Right: MFR = 4.0 kg/s

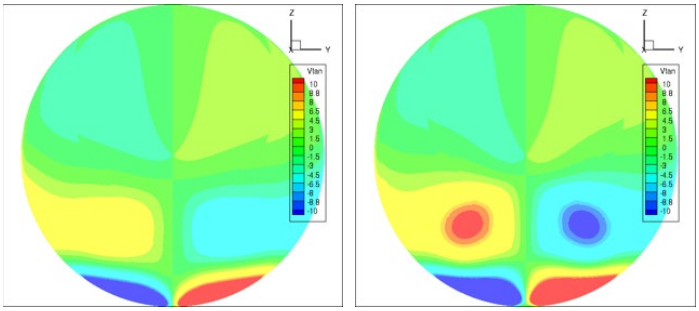

Figure 16 – Tangential velocity at fan face.

Left: SA-RC. Right: SA-QCR2000

The angle α_i is computed by using the axial and tangential velocities at a particular point. The ratio of these two velocities is an interesting parameter to measure the homogeneity of the flow. Figure 14 shows the variation of this parameter as function of the azimuthal position of the measured point. A swirl intensity of 0 represents a totally axial flow, and consequently, a less distorted flow. The outer rings, represented by the blue and the red colors in the swirl profile, have the highest swirl intensity value. As expected, highest values of this term are found in the regions affected by the ingestion of the boundary layer, and in the conditions in which its negative effects are most evident. These regions are areas where axial velocities are lower, which are influenced by the thickness of the boundary layer and, in some cases, by the separated flow. Furthermore, tangential velocities in these regions increase due to the location of the vortices. Figure 15 shows the axial velocity field and the vortices positions at fan face. By comparing the intensity plot obtained by the two cases it is possible to highlight two physical phenomena. First, the axial flow homogeneity variance according to the MFR value. For a high value of MFR the homogeneity are better, the opposite occurs with a low value of MFR. Second, the vortex position an intensity can be deducted by the maximum swirl intensity. The intensity of the vortex plays a key role in distortion criteria. The vortex core displacement shown in figure 15 are also detectable in the swirl intensity plots shown in figure 14. Figure 16 shows the tangential velocity.

In this document the **Mean SI**, based on swirl intensity parameter, is analyzed. This parameter simply takes the SI_i mean value as distortion parameter. Figure 13 shows its value for each turbulence model as function of the mass flow rate. When there is no separation (between *MFR* = 3.6 and 4.0 kg/s) all turbulence models give very similar values. When the separation appears (for *MFR* between of 3.4 and 3.6 kg/s) the mean SI values predicted by the SA-QCR2000 model are larger, which could be linked to the early detachment predicted by this model. In cases where there is a separation (between *MFR* = 3.4 and 3.0 kg/s) this value tends to increase inversely with MFR. There is a notable difference between the values obtained from the SA family solutions and the solutions predicted by the other models. This could mean that this distortion criterion has a high sensitivity to the predicted solution for each model.

V. Proposition of new BLI distortion indices

The aerodynamic distortion on a BLI engine is clearly affected by both pressure losses and swirl velocity. It is very likely that a distortion criterion suitable for BLI configurations needs to take into account both parameters. Therefore, a first attempt to provide a more adapted distortion index based on a mixture of both parameters is proposed. This index is called VPDI (Velocity and Pressure Distortion Index). Its value is computed following Equation 4.

$$VPDI = max\left(\int_0^{2\pi}\left[\left(|\boldsymbol{\alpha_j}|+\mathbf{1}\right)-\frac{\boldsymbol{Pt_j}}{\overline{\boldsymbol{Pt}}}\right]\boldsymbol{d\theta}\right) \qquad \textbf{Equation 4}$$

$\boldsymbol{\alpha}$ is an angle which take into account the ratio between the axial velocity and tangential velocity. Its value is calculated in equation 3. $\boldsymbol{Pt}$ is the total pressure. The subscripts *j* indicate where this angle/pressure is calculated. In the first instance, those parameters can be calculated along a measured ring. In this case the ring is discretized in *i* positions. The *i* and *j* positions are shown in figure 9. The distortion criteria value is the maximum value between the *j* rings.

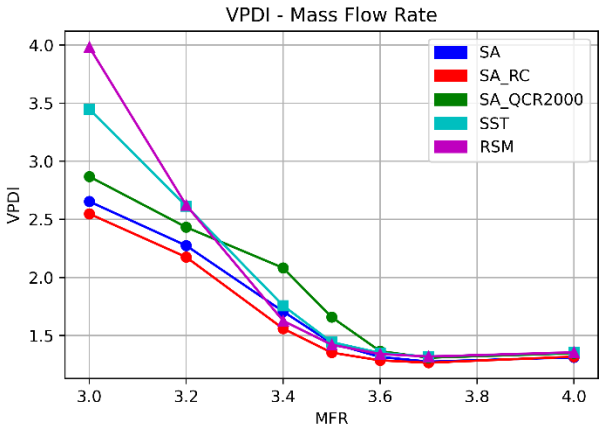

Figure 18 - VPDI variation with MFR

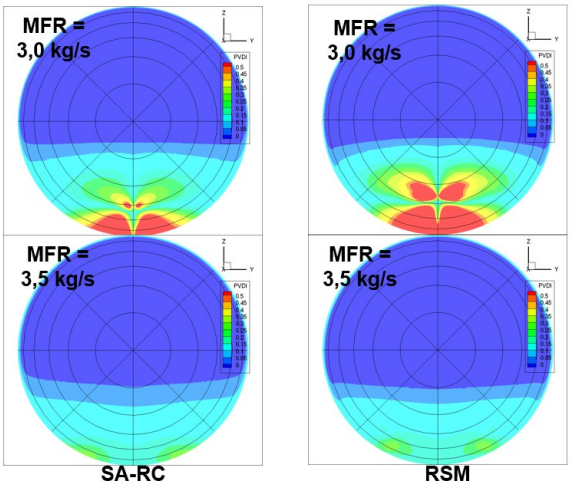

Figure 17 - VPDI value at fan face.

Left: SA-RC model. Right: RSM model.

VPDI takes the integral of a variable that depends on a velocity term and a pressure term. When there are pressure losses the term on the right tends to decrease. When the ratio of tangential and axial velocity increases, the velocity term increases too. At lower MFR values, the VPDI value tends to predict a higher distortion. This higher value is linked to the pressure losses and tangential velocities. Radial and tangential velocities tend to be weaker with higher MFR values, contrary to the total pressure, which is always affected even at high MFR. Figure 18 shows this term calculated in some simulation cases.

This distortion index tends to predict a similar behavior as the one obtained with distortion criteria only based on swirl parameters. The only advantage shown by the *IDC*, to locate when the detachment occurs, is less evident in the proposed criterion.

$$\boldsymbol{\beta IDC} = \boldsymbol{MAX_{i=1}^{nradius-1}}\left(\mathbf{0.5}\left[\frac{\left(\overline{\beta_i}-\overline{\beta min_i}\right)}{\overline{\beta_f}}+\frac{\left(\overline{\beta_{i+1}}-\overline{\beta min_{i+1}}\right)}{\overline{\beta_f}}\right]\right) \qquad \textbf{Equation 5}$$

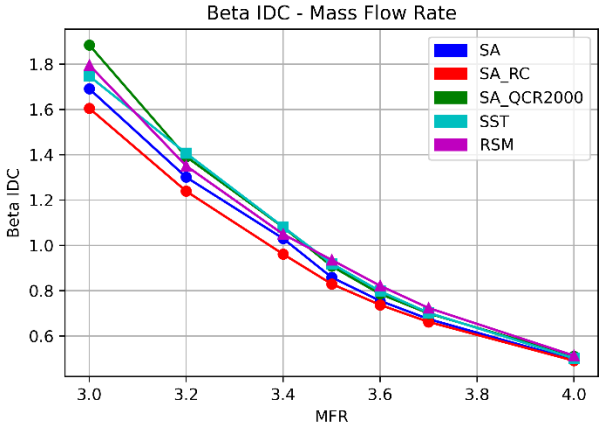

Figure 19 - βIDC variation with MFR value

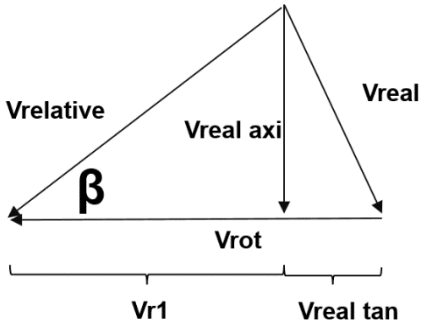

Figure 20 - Velocity triangle

Another research direction would be to take the advantage of velocity-based distortion criteria to assess the homogeneity of the angle of attack perceived by the fan blades. A first approach has been done using the velocity triangle, as shown in figure 20, to calculate this angle for a generic fan. A generic *Vrot* is used as the rotation velocity of the fan. Vreal is the velocity perceived by the intake affected by the boundary layer. Finally, the angle β is the angle created between the rotation velocity vector and relative velocity vector. The mathematical approach for this index is based on the IDC formulation, shown in Equation 5. This formulation highlights the angle of attack changes along the rotation of the blade.

Figure 19 shows the behaviour of this distortion index in relation with the MFR. It can be observed that the distortion predicted by this index increases when the MFR value decreases. This result shows some relation with the negative effects of the BLI configuration, however, it is not possible to clearly identify for which MFR values separation appears.

Several authors have made similar approximations to characterize the distortion [16] [17]. However these approximations are more oriented to evaluate the impact on the operation of the engine and not on the characterization of the flow behaviour.

VI. Partial conclusions and work perspectives.

Some of the distortion indexes classically used in the industry have been analyzed on a academic BLI configuration. The main objective of computing distortion indices is the analysis of the physical phenomena present in the flow and their subsequent impact on the distortion so as to provide a driving parameter to design engine components.

Given this premise, and applying it to a BLI engine design, it can be concluded that *DC(60)* index does not highlight the flow physics. The evolution of this parameter cannot discriminate between a separated flow and an unseparated one. Regarding the pressure-based distortion criteria, the most promising index so far is the *IDC*, which exhibits an interesting correlation between the flow behavior and its value. The maximum value corresponds to the mass flow rate value for which a separated flow appears.

So far, the velocity-based distortion criteria seem to be more appropriate than the pressure-based ones to characterize the distortion in a BLI configuration. The proposed distortion criteria show a big distinction between attached and detached flow cases. Furthermore, there is a clear difference in behavior between the one-equation and two-equation RANS models, in addition to great differences perceived between turbulence models which use a first-

order or second-order closure model, and a full Reynolds Stress Model. These conclusions provide a way forward for research into distortion indices. It is planned to investigate the velocity-based distortion indices even further in addition to considering engine performance and operating parameter impacts.

New distortion indices have been proposed to assess the distortion for BLI configurations. First, mixture of both pressure and velocity parameters is interesting, since they are the main physical phenomena that affect distortion in this type of configurations. The VPDI is only a first approach, more work needs to be done on this type of distortion criterion in order to achieve a real breakthrough with respect to usual distortion indices. *βIDC* proposes an interesting way to couple distortion at engine intake and the relative angle of attack perceived by the fan. Although this index shows disadvantages with respect to other more traditional ones, it leads to think about another way to link the flow behaviour at the intake, and also to predict the impact on the engine response. An energetic analysis, taking the work done by the fan to re-homogenize the flow might be an interesting analysis to complement this research direction.

Acknowledgment

The authors would like to acknowledge Airbus and ONERA colleagues for their advice and assistance throughout the process. The authors would like to thank the French National Agency for Research and Technology (ANRT) and Airbus for financial support of this study.

References

1. **B, Yutko, et al.** Conceptual Design of a D8 Commercial Aircraft. 17th AIAA Aviation Forum, AIAA 2017-3590, 2017.

2. **Drela, M.** Development of the D8 Transport Configuration. 29th AIAA Applied Aerodynamics Conference, 2011.

3. **Wiart, L., Atinault, O., Grenon, R., Paluch, B., and Hue,D.** Development of NOVA Aircraft Configurations for Large Engine Integration Studies. 33rd AIAA Applied Aerodynamics Conference, 2015.

4. **Lucas, J. R., O'Brien, W. F., & Ferrar, A. M.** Effect of BLI–Type Inlet Distortion on Turbofan Engine Performance. Volume 1A: Aircraft Engine; Fans and Blowers. 2014.

5. **Gray, J. S., Mader, C. A., Kenway, G. K. W., & Martins, J. R. R. A.** Coupled Aeropropulsive Optimization of a Three-Dimensional Boundary-Layer Ingestion Propulsor Considering Inlet Distortion. Journal of Aircraft, 1–12, 2020.

6. **Florea, R. V., Voytovych, D., Tillman, G., Stucky, M., Shabbir, A., Sharma, O., & Arend, D. J.** Aerodynamic Analysis of a Boundary-Layer-Ingesting Distortion-Tolerant Fan. Volume 6B: Turbomachinery, 2013.

7. **SAE Aerospace Information Report**, A methodology for assessing inlet swirl distortion, Society of Automotive Engineers, Warrendale, PA, AIR 5686, 2010.

8. **Cambier, L., Heib, S., and Plot, S.**, The Onera elsA CFD software: input from research and feedback from industry, Mechanics & Industry, Vol. 14, No. 3, pp. 159-174. 2013

9. **Shur, M. L., Strelets, M. K., Travin, A. K., Spalart, P. R.,** Turbulence Modeling in Rotating and Curved Channels: Assessing the Spalart-Shur Correction. AIAA Journal, 2000. Vol. 38, No. 5, pp. 784-792. 2000.

10. **Spalart, P. R.,** Strategies for Turbulence Modelling and Simulation.International Journal of Heat and Fluid Flow, 2000. Vol. 21, pp. 252-263. 2000.

11. **Hanjalić K. and Launder B.**, Modelling Turbulence in Engineering and the Environment: Second-Moment Routes to Closure, ISBN 978-0521883986, Cambridge University Press, 2011.

12. **Spalart, P. R. and Allmaras, S. R.,** A One-Equation Turbulence Model for Aerodynamic Flows, Recherche Aerospatiale, No. 1, pp. 5-21. 1994.

13. **Menter, F.R.,** Two-Equation Eddy-Viscosity Turbulence Models for Engineering Applications. AIAA Journal, 1994. Vol. 32, No. 8, pp. 1598-1604. 1994.

14. **Eisfeld, B., Rumsey, C., & Togiti, V.,** Verification and Validation of a Second-Moment-Closure Model. AIAA Journal, Vol. 54, No. 5, pp. 1524–1541. 2016.

15. **Technical Committee S-16.** Inlet Total Pressure Distortion Considerations for Gas Turbine Engines. 1983.

16. **Miller D, Wasdell D**. Off-design prediction of compressor blade losses. IMECHE C279/87; 1987

17. **Valencia, E., Hidalgo, V., Nalianda, D., Laskaridis, P., Singh, R.,** Discretized Miller approach to assess effects on boundary layer ingestion induced distortion. Chinese Journal of Aeronautics. Vol 30, pp. 235-248. 2017